Distribution Agreement

In presenting this thesis as a partial fulfillment of the requirements for a degree from Emory University, I hereby grant to Emory University and its agents the non-exclusive license to archive, make accessible, and display my thesis in whole or in part in all forms of media, now or hereafter now, including display on the World Wide Web. I understand that I may select some access restrictions as part of the online submission of this thesis. I retain all ownership rights to the copyright of the thesis. I also retain the right to use in future works (such as articles or books) all or part of this thesis.

Daniel Glodener March 25, 2019

Age-Related Morphological Changes of Cortical Thin Unmyelinated Axons in Mice

by

Daniel Glodener

Morten Raastad, MD, PhD
Adviser

Neuroscience and Behavioral Biology

Morten Raastad, MD, PhD
Adviser

Patrick Cafferty, PhD
Committee Member

Keith Easterling, PhD
Committee Member

2019

Age-Related Morphological Changes of Cortical Thin Unmyelinated Axons in Mice

by

Daniel Glodener

Morten Raastad, MD, PhD

Adviser

An abstract of
a thesis submitted to the Faculty of Emory College of Arts and Sciences
of Emory University in partial fulfillment
of the requirements of the degree of
Bachelor of Sciences with Honors

Neuroscience and Behavioral Biology

2019

Abstract

Age-Related Morphological Changes of Cortical Thin Unmyelinated Axons in Mice

By Daniel Glodener

Cognition undergoes radical age-dependent change throughout life. Behind those cognitive changes are morphological ones. The brain loses weight, grey matter shrinks, and some populations of neurons decrease in number (Svennerholm 1997; Terribilli 2011; Terry 1987). In parallel, neurons change with age in the cortex, with lower firing rates in hippocampal neurons and neuronal pathology mirroring aging cells throughout the body (Geinisman 1986; Phillip 2017). The structures of hippocampal and neocortical neurons have been thoroughly studied, but data regarding features of the longest and most abundant component, the axon, remains sparse. The thin axons that project from these cells and comprise most of grey matter have a typical structure. Defining features of these typical unmyelinated axons (TUAs) are thin unmyelinated shafts, *en passant* boutons down the length of the shaft, and excitatory synapses with dendritic spines. The organization of these features, such as bouton spacing, influences the arrangement of neuronal connectivity. Although patterns of TUA structural organization have been observed they are poorly understood, and very little is known about the changes in these patterns. We hypothesized that normal aging would correlate with changes in commonly observed morphological features, including inter-bouton interval (IBI), the spatial distribution of boutons, and bouton size. We used fluorescent microscopy with DiI labelling to image TUAs in mice and measure these variables of morphology. Here we show that morphological change can be predictable in TUAs, depending on the location of the axon. Axons were similar in mean IBI and spatial variability but differed in bouton size. Hippocampal axons decreased in IBI and increased in bouton size with age, while neocortical axons showed no significant morphological change with age. We also explore various labelling methods to determine their advantages and disadvantages.

Age-Related Morphological Changes of Cortical Thin Unmyelinated Axons in Mice

by

Daniel Glodener

Morten Raastad, MD, PhD

Adviser

A thesis submitted to the Faculty of Emory College of Arts and Sciences
of Emory University in partial fulfillment
of the requirements of the degree of
Bachelor of Sciences with Honors

Neuroscience and Behavioral Biology

2019

Acknowledgments

I would like to thank Dobromila Pekala for her assistance early in my research experience and contribution of prior data. I would also like to thank Dina Yakout and Danielle Hopkins for their prior data contributions. I am grateful to Leah Roesch and my committee members for their guidance. I extend my gratitude to Marie-Claude Perreault, Renee Shaw, Michael Sawchuk, and Kenyatta Gray for their technical support.

Table of Contents

Introduction

By 2060, the American population over the age of 65 will grow to approximately 24 percent of the total population from 15 percent in 2014 (Colby and Ortman 2015). As this population increases, it becomes even more important to understand the physiological changes of the brain that occur across the lifespan and their resulting cognitive effects. Studies demonstrate a significant linear decline in processing speed, working memory, and free recall associated with normal aging (Dobbs and Rule 1989; Park 1996; Salthouse 2009; Witte 1990). In humans without neurodegenerative disease aging contributes to significant morphological changes in the cortex, such as a 20 percent loss of brain weight from 20 years of age to 100 years of age and volumetric reductions of grey matter in the hippocampus and frontal regions of the neocortex (Jernigan 2001; Svennerholm 1997; Terribilli 2011; Terry 1987). Functional changes, like reduced activity in the subiculum and dentate gyrus, are also present in older adults without neurodegenerative disease (Small 2002). Gross structural and functional changes of the cortex occur parallel to microscopic changes. For example, hippocampal pyramidal cells of older rats have reduced firing rates and fewer muscarinic receptors and lose axospinous synapses in the dentate gyrus (Geinisman 1986; Lippa 1981). Knowledge of cognitive development in early age is also accumulating. Simultaneous structural changes of the cortex in early life, such as the increase in the proportion grey matter in childhood, may help explain the mechanisms of cognitive growth (Courchesne 2000). Cellular changes, such as the pruning of dendrites in the dentate gyrus and the increase in spine density from pre- to late-pubertal hamsters, may also link to gross structural and cognitive changes (Zehr 2008). Building on the current knowledge of morphological changes augments our understanding of how the mind develops and changes over the lifespan. While much has been discovered about cellular changes of the developing,

maturing, and senescing nervous system, little is known specifically about the changing structure of thin unmyelinated grey matter axons, which comprise over 50% of the volume of grey matter in rat cortex (Mishchenko 2010). The substantial presence of this type of axon in the cortex signifies a great need to study them further.

Age-related changes in physical cell properties such as greater cell shape irregularity and biophysical variability (e.g. increased mechanical stress and cytoplasmic stiffness) have been observed in human dermal fibroblasts (Phillip 2017). Changes of a similar nature occur in neurons. There are considerable data regarding age-related morphological and functional changes to the peripheral nervous system. Chase and others (1992) show that in cats there is an age-dependent reduction of axonal diameter and myelin thickness in the masseter nerve. Electrophysiological analysis indicates that this decrease in diameter leads to slower conduction velocities, which may be the source of degenerated jaw function. After the age of 60, myelinated and unmyelinated axons tend to decrease in density in the sural nerve of humans with an increase in variability of internodal length and axon diameter (Jacobs and Love 1985). Small unmyelinated axon fibers of the pelvic nerve decrease significantly in number in aged rats (Nakayama 1998). Unmyelinated C-fiber axons in the skin of older humans with a mean age of 56 show hypoexcitability, decreased conduction velocity, and longer velocity normalization periods after high frequency stimulation, believed to be caused by reduced sodium-potassium pump activity which is likely due to slowing axonal transport (Namer 2009; Verdu 2008). The age-related pathologies demonstrated by these studies vary by cell type and location but show significant change in the structure and function of the peripheral nervous system. Hippocampal neurons of aging rats also have increased activity of the cellular senescence marker beta-galactosidase (Geng 2010). Since morphological changes in axons of the peripheral nervous

system are commonly observed and hippocampal axons share biochemical markers of aging with other cells, significant morphological changes may also arise in cortical grey-matter axons of the central nervous system. Studying these changes could provide insight into the mechanisms behind shifting and declining cognitive function and reveal potential therapeutic targets.

Unmyelinated grey-matter axons are extremely abundant in the cortex, forming an expansive network between neurons. The 2010 ultrastructural electron microscopy study done by Mishchenko and others shows that 60% of hippocampal cell membrane in rats is comprised of thin unmyelinated axons (TUAs). A single cell in the CA3 area of the hippocampus can have axonal projections totaling up to 300mm in length and can make synapses with up to 60,000 other neurons (Li 1994). Action potentials initiated in CA3 pyramidal cells can conduct across distances around 2 millimeters (Raastad and Shepherd 2004). Considering the extensive network of a single neuron, pathology of the axons that affects characteristics of action potentials could cause errors or alterations in action potential propagation to distal connections. Information regarding structural features integral to neuron function like the distribution and size of varicosities (synaptic boutons) is relevant to understanding both how interactions between neurons change and the effect those changes have on cognition.

A fundamental idea in physiology is that structure determines function. Accordingly, an axon's function is determined by its geometry. For example, both the diameter of an axon and the presence of boutons affect action potential propagation velocity (Manor 1991). TUAs tend to have *en passant* boutons along their paths. *En passant* boutons are synapses that occur along the length of the axon that make synapses with one or more dendritic spines. These boutons are distinct from *terminaux* boutons, which occur at axons terminals and form synapses typically with dendritic shafts but occasionally dendritic spines (Anderson 2001; Gorolla 2017). Most

TUAs of the hippocampus have a relatively small diameter of 0.17μm, meaning that their surface area to volume ratio (S/V) is much higher than other axons (Shepherd 1998). A higher S/V leads to higher intracellular concentrations of ions after action potentials compared to larger axons. A specific number of ions need to be displaced into the cytoplasm in order to change membrane voltage a given amount. If the cytoplasmic volume of the cell is small relative to the membrane surface area, there will be a larger change in the ion concentration gradient. A simulation performed by our lab explored aspects of diffusion in these axons, which along with Na/K pumps helps restore the ion gradient to homeostatic levels. Boutons, which reduce the S/V in unmyelinated axons, help restore the ion gradient through diffusion from the shaft into larger bouton volumes with lower total ion concentration. If a given axon segment has regularly spaced boutons, all the between-bouton midpoints of the shaft will return to homeostatic ion concentrations after an action potential at the same rate. If the same segment had the same boutons randomly spaced, midpoints between boutons of a greater interval would diffuse to homeostatic levels more slowly than those in shorter intervals, creating bottlenecks that increase the total time of diffusion. Variability in bouton size affects diffusion as well. Larger boutons provide a larger cytoplasmic volume and thus a lower ion concentration after an action potential, which accelerates diffusion into the bouton and alleviates diffusion slowdown further down the shaft. If the size and spacing of boutons change in variability or magnitude, the sustainability and velocity of action potentials would be affected. An axon with smaller and more randomly spaced boutons may be able to fire action potentials at the same frequency of an axon with large and equally spaced boutons but would be slower to recover from hyperpolarization, limiting how long it could fire at an identical frequency until failure. Diffusion is also relevant to other aspects of neuronal function, including ATP transport and movement of proteins (Coleman 2005). Over

half of the boutons along the shafts of hippocampal CA1 and CA3 axons do not contain mitochondria (Shepherd 1998). Impaired diffusion could be damaging to the overall health of the axon, as segments that are distant from boutons containing mitochondria would have slower influx of essential ATP. The spatial distribution and size of the boutons are critical to an axon's physiology, motivating our main goal of finding trends in morphology that may affect overall function.

Our current objective is to examine the morphological changes with age of the *en passant* boutons of thin unmyelinated grey matter axons in mouse hippocampus and neocortex, focusing on inter-bouton interval (IBI) and bouton size relative to the axonal shaft. By measuring the IBI and relative contrast, we can observe potential cortical neuropathies that may affect the ability of these neurons to propagate action potentials.

Alongside examining axon morphology, another objective of this study is to explore sample preparation methodology. Current techniques are adequate for study but have the potential to be improved, particularly in the reduction of background emission which increases the noise to signal ratio of data. In this study we use DiI to fluorescently label axons so we can measure aspects of their morphology (Figure 1). DiI was chosen because it is a widely-used lipophilic, fluorescent carbocyanine dye that is simple to use and effectively diffuses through the lipid membrane of cells, brightly labeling neurons and their projections (Honig 1986). DiI can sparsely label axons depending on how it is applied, which is crucial for studying axon morphology. Histochemistry studies using DiI are typically done using samples fixed with paraformaldehyde (PFA) solutions at concentrations of 1.5%, 2%, and 4%. Fixation of mouse hippocampus at 4% PFA limits fluorescent dye diffusion and produces strong background emission through autofluorescence, while lower concentrations of 1.5% and 2% yield efficient

dye diffusion and reduced background emission (Cheng 2014). 4% PFA also causes a 62% volume shrinkage of mouse brain, potentially altering the dimensions of axons (Wehrl 2015). Other potentially viable fixation chemicals are sodium azide, which helps with structural and mitochondrial preservation while preventing bacterial growth, and potassium permanganate, which

has been used for preserving tissue for electron microscopy (Minassian 1979; Todd 1981). Using these chemicals could lead to similar issues encountered when using PFA but to a different degree. Degradation of fresh tissue is a concern when conducting morphology studies but using fresh tissue does present some advantages. Dyeing fresh samples may speed up dye diffusion and eliminate background emission altogether without altering the original morphology of axons, and the time interval between tissue harvesting and imaging would be at least 24 hours shorter. Finding an efficient and reliable method is necessary to gather the large amount of data required for related studies.

Materials and Methods

Animals: All animal procedures were in accordance with Emory Institutional Animal Care and Use Committee regulations. Subjects were ICR wild-type mice at least 2 weeks old with no upper limit on age.

Sample Extraction and Preparation: The mice were anesthetized by exposure to 5mL of isoflurane, decapitated, and their brains cut in half along the longitudinal fissure and immediately extracted and placed into ice-cold PBS solution. If the sample was to be fixed, the brain was placed in preservative solution and stored in a refrigerator for 24 hours prior to slicing.

Preservative solutions were either 3% or 1% paraformaldehyde, 1% sodium azide, or 0.1% potassium permanganate.

Slicing: The slicing procedure began either as quickly as possible following brain harvesting for fresh samples or after 24 hours in refrigerated preservative fluid for fixed samples. The brain was stored in fresh PBS solution on ice while 50 mL of 1.2% agar solution was prepared on a hot plate. One round sheet of filter paper was soaked with PBS and dried by pressing between a paper towel to prevent warping, then secured to a large petri dish with wax. A small layer of agar was poured on the filter paper and dried to create a platform. Both brain halves were placed in parallel on the agar platform, and lukewarm agar was poured layer by layer to securely encase the samples. The petri dish containing the agar-encased brain was secured to the slicing device using two small mounds of dental wax. The slicing device (Figure 2) is an acrylic platform that can be moved in 10 μm increments by a screw mechanism. A safety razor blade is attached to two aluminum blocks screwed together, creating a cutting tool with adjustable blade height and angle. The tool is placed on the platform and moved steadily down by hand. This allows for straight, precise cuts. The tip of the cutting edge was adjusted to just below the agar platform for complete cuts, and the brain sliced in 200μm thick slices. Slices were carefully extracted with a wide-tipped pipette and placed in a PBS-filled glass petri dish resting on a bed of ice.

Dyeing: Fluorescent, lipophilic DiI crystals (Thermo Fischer Scientific, Eugene, OR, USA) were prepared by placing an approximately 1.5mm wide pile on a glass slide, suspending in two drops of distilled water, and crushing with a palette knife. The crushed crystals were rinsed from the slide into a plastic test tube and filled with deionized water to a total volume of 50mL, then sonicated for 1 hour to break them down further into smaller fragments. The crystal

solution was then vacuum filtered through either a 3µm or 0.45 µm Millipore filter to yield appropriate crystal sizes left behind on the filter. Eliminating small crystals significantly reduced background labelling and emission. The filtrate containing smaller crystals was discarded. The Millipore filter was placed on filter paper resting on a bed of paper towels in a glass petri dish to promote draining. The slices picked up from the PBS solution using a wide-tipped glass pipette and placed onto the Millipore filter surrounded by PBS. Care was taken to ensure the slices remained hydrated. The paper towels and filter paper drained the fluid surrounding the slices and suctioned them slightly into the Millipore filter. This helped the crystals embed into the slices, allowing them to contact and diffuse through the lipid membranes of the axons. The entire filter with the slices was dunked into a beaker of cold PBS and the slices removed with gentle squirts from a small pipette. The slices were gently picked up with the wide-tip pipette and placed into a container with cold PBS solution and immediately refrigerated. All instruments were thoroughly cleaned with 90% isopropyl alcohol after the procedure to remove any remaining DiI, preventing contamination that would show up as background fluorescence in imaging.

Mounting: After 24 hours of refrigerated storage, the samples were collected with the wide-tipped pipette and placed on a small spoon. The surrounding liquid was dried with a paper towel and the slice submerged in glycerol. The slice was then slid off the spoon into a drop of glycerol on a microscope slide rather than scooped and placed, which prevented damage from rough handling and smearing from unabsorbed crystals on the viewing side of the slice. Cover glasses were mounted using a paste for sturdier slide construction, which prevented squeezing of the sample and movement during imaging. One part dental wax and two parts petroleum jelly were melted together and cooled to produce a mounting paste with ideal malleability. An ideal paste was soft enough to manipulate and apply to the glass easily, but sturdy enough to provide

adequate structural support to bolster the glass where it would not move from the level it was placed. Six small dabs of the mounting paste were applied with a thin-tipped palette knife to the rectangular cover glass, one on each corner and one on the midpoint of each length. The cover glass was place above the sample, and gently pressed by the corners until it touched the top of the sample without putting pressure on the slice and flattening it (Figure 2).

Imaging: Sample slides were viewed on either of two confocal microscopes, a Nikon Eclipse E-800 using the image software Neuroleucida or a Keyence BZ-X710 with its native software. The hippocampus was located using transmitted light and 4X magnification. A Chroma Cy3 filter set producing excitation light with a wavelength spectrum of 530-560nm was used in the Keyence for fluorescent imaging, and a Nikon G-2A Cy3 filter set producing excitation light of 510-560nm was used in the Nikon. Image stacks of the axons taken using at the maximum magnifications of 60X with the Keyence and 100X with the Nikon. Axons were chosen based on homogeneity of structure, brightness of background noise, parallelism to the focal plane, and strength of emission. Image stacks were typically 5-7 μm in length along the z-axis and were taken in 0.5 μm increments. To reduce photobleaching in the Nikon, filters that dampen excitation light were used extensively, and images were taken with low light and high exposure time rather than high light and low exposure time. The Keyence included a low-photobleaching mode, which turned off excitation light until needed.

Image processing: Using the photo analysis software ImageJ, the stacks were treated with a median contrast filter to subtract background noise, transformed to a maximum intensity z-projection, and converted to a 16-bit format for ease and accuracy of analysis (Figure 3a-d). Contrast intensity profiles (Figure 3, Figure 4) were taken of TUAs in projections of acceptable quality by highlighting the axon in ImageJ with a 2.2μm thick line and extracting contrast values

along that line. Higher quality images were those with dark backgrounds, bright and even fluorescence, long length, and few or no intersecting axons. The profiles were first normalized in the following way to allow for relative analysis rather than absolute value analysis. A fitted 2nd degree polynomial was subtracted from the plot to flatten it so that nadirs had an approximately equal value, which represented the relative contrast/size of the axonal shaft. All values of the plot were then divided by the median nadir value to normalize the axon shaft value to 1. To decompose the plots to analyzable data, boutons were identified by fitting a gaussian function to every peak. Peaks qualified as boutons if they were at least twice the magnitude of adjacent nadirs. Axons must have had at least 3 boutons to be considered for analysis. The mean and coefficient of variation (CV=standard deviation/mean) for IBIs were determined from the normalized decomposition, with IBI measured in microns as the distance between representative peaks in the profiles. Bouton size was estimated as the mean of the integral values of each bouton in the axon profile. The integral for each bouton was averaged, providing a value that represented size of the boutons relative to the axon shaft.

Results

A total of 79 neocortical axons from 11 fresh mice, 3 hippocampal axons from 1 fresh mouse were used. 416 hippocampal axons from mouse brains preserved in PFA and analyzed using the same methods in our lab's prior studies were also used in statistical analysis.

Axon IBI, CV, and Bouton Size

There was a significant negative correlation between age and IBI ($r = -0.148$, $p = 0.003$, Figure 5) in hippocampal axons from PFA-preserved tissue. The CV for IBI ($r = -0.038$, $p =$

0.435) showed a non-significant negative trend. There was a significant positive correlation between age and bouton size ($r = 0.142$, $p = 0.004$). The mean IBI for hippocampal axons was 4.5µm with a standard deviation of 1.3µm.

A fitted exponential curve on a scatter plot containing mean IBI values for all hippocampal axons shows a decline in IBI change (Figure 6). The mean IBI decays by approximately 36.8% every 27.25 days of age as indicated by tau.

Figure 7 shows axon profile autocorrelations of hippocampal axons from young and old mice as functions of spatial lag. Old mice are defined as older than 200 days old and young mice are defined as younger than 100 days. The graphs demonstrate that the relationship between the presence of boutons and distance from the previous bouton in older mice transitions from a negative correlation to a random relationship at shorter intervals of distance.

Cortical axons from fresh tissue did not show a significant correlation between age and IBI ($r = 0.176$, $p = 0.121$, Figure 8) or bouton size ($r = -0.169$, $p = 0.137$), however, there was an upward trend with IBI and downward trend with bouton size. The CV for IBI ($r = 0.196$, $p = 0.084$) showed a non-significant upward trend. The mean IBI was 6.12µm with a standard deviation of 1.61µm.

Preservation Methods and Microscope Choice

Both microscopy image and tissue quality of samples preserved with 3% PFA, 1% sodium azide, and 0.1% potassium permanganate were analyzed visually. Potassium permanganate dyed the slices a deep purple and severely compromised their structure, eliminating any possibility of fluorescent imaging. Sodium azide preservation produced slices that looked similar to fresh slices. PFA slightly shrunk and hardened the slices. Fluorescent

images produced by sodium azide had a significant background emission. The axons did not absorb DiI well enough to illuminate the entire axon, restricting the viability of axon analysis. PFA produced the best images out of the three preservation methods, with relatively low background emission and axons that absorbed DiI well enough to completely illuminate the axons. Fresh slices produced the highest quality images, with minimal background emissions and axon labelling of a similar quality to PFA (Figure 9). The process to create imageable slides was 24 hours quicker for fresh slices than preserved slices.

The Nikon E-800 was ideal for imaging. The excitation emission wavelength of its filter seemed to be better suited for DiI, producing clearer images of the axons. The Keyence BZ-X710 produced lower clarity images of axons with slightly more background emission (Figure 10a). The 100X magnification of the Nikon lens produced larger images of axons than the 60X lens of the Keyence, however the Keyence had a higher native resolution.

Discussion

The main findings, which include both my data and data gathered previously by members from my lab, are that the morphology of thin unmyelinated axons (TUAs) in the hippocampus varies with age and between axons of the same animal. The characteristics of axons in the hippocampus are similar to those in the cerebral cortex, but changes of these characteristics were not found. This could be due to a much lower sample size of neocortical axons. Findings regarding methodology are that while the use of fresh tissue yields better images and quicker data production, paraformaldehyde fixation yields images that are adequate for data analysis and causes no significant change to the morphology of the axons.

Significant Change in IBI, CV, and Bouton Size of Hippocampal Axons

Using a linear regression model, we found that mean inter-bouton interval (IBI) decreases with age in hippocampal axons of mice. This finding is the first to determine a change correlated with age of the spatial distribution pattern of boutons in grey matter TUAs. The mean IBI for all hippocampal axons averaged to 4.5μm, consistent with other findings of 3-5μm and 3.0μm for hippocampal axons (Andersen 1975; Shepherd 1998). Although there is a lack of information directly regarding the age-related changes of IBI, synapse density can be used as an approximate predictor of IBI. It has been found that 75% of synaptic axonal *en passant* boutons in the hippocampus make a single synapse with a dendritic spine, and the remaining 25% have multiple synapses (Sorra 1993). Another study found that 13% of all axonal boutons made no synapses, 68% made one, 19% made two or more (Shepherd 1998). Since the majority of *en passant* boutons are synaptic, synaptic density can be used to estimate how many boutons occur in a given space of hippocampus, giving some insight into IBI. IBI is also used as a variable for the estimation of the number of potential synapses along the length of a dendrite, further supporting the following comparison between IBI and synaptic densities (Stepanyants 2002). Several studies have observed similar age-related patterns of synaptic density. Mature mice (39 days and older) have a greater number of dendritic spines per spine length in the hippocampus than younger mice (22 days and younger), with every spine forming a synapse with axonal boutons (Kirov 1999). Along with axon length and density, larger number of synapse-forming dendritic spines could be an indicator of higher presynaptic bouton density, representing a lower IBI. The number of synapses in the hippocampus does not change with age, except for in the dentate gyrus and in CA3 cells of the stratum lacunosum moleculare (Adams 2010; Geinisman 1992; Geinisman 2004; Peters 1996). It is therefore possible that the change in IBI we observed reflects a redistribution rather than a net

addition of boutons. However, stimulation of Schaffer-Collateral axons in older mice produces weakened excitatory post-synaptic potentials, indicating either fewer synapses or weaker function of synapses (Barnes 2000). Considering prior evidence that net synapse number does not change, it is more likely that synapses become weaker or non-functional with age. Decreased IBI in aged mice may be a mechanism of compensatory function to maintain the strength of afferent connections, as boutons that are closer together are more likely to make connections to the same dendrite. Axons with varicosity structures similar to those found in TUAs have been observed to change IBI as a physiological response to stress. Varicose axons in the periaqueductal gray matter of rats that underwent stress show an increase in varicosity density (Smalls 2012). This supports the ideas that IBI can change and, if normal aging were considered a biologically stressful or pathological process, that senescence could decrease IBI. Since age correlates with reduced hippocampal function in normal aging (Small 2002), the decrease in IBI could be either a homeostatic response to pathological processes occurring at the neuronal level or a pathological process itself.

A beneficial consequence of decreased IBI would be increased rates of diffusion, mitigating the scarcity of resources in boutons brought about by their isolation along the axon and assisting in the restoration of ion concentration gradient after action potentials. This follows the supposition that IBI is a response to neuronal pathology.

An exponential model fitted to the same data reveals that IBI decreases most rapidly between 2-3 months of age, with a milder decrease after 100 days of age. Although data from younger mice is more plentiful and thus has a much stronger effect on the model than older mice, it still illuminates a strong trend in early age. The *en passant* boutons in similar axons from pyramidal cells of the barrel cortex are largely stable in mature mice, but axonal boutons have a

higher turnover rate and a net loss from 1 to 2 months of age (Qiao 2015). Due to the lack of information regarding bouton stability in the hippocampus and considering the homogeneity of TUA characteristics, these findings in the neocortex will have to suffice for an estimation of hippocampal bouton stability. Increased bouton stability would drive down IBI as bouton density does not decrease as readily. If the axons of pyramidal cells in the hippocampus have a similar bouton loss timeframe as neocortical axons, this finding supports our conclusion of more rapid decrease of TUA IBI in early age. As for a more direct comparison, the trend we observe in IBI matches that of hippocampal neurogenesis. In mice, the rate of neurogenesis in the hippocampus decreases exponentially with age (Lazic 2012). An exponential decrease is also found in humans, from 3 to 6 months of age (Knoth 2010). The matching trend of change of neurogenesis in the hippocampus could be a clue about the mechanism behind the mean IBI trend. New axons would have fewer synapses than established axons, thus fewer boutons and higher IBI. Additionally, as described above, boutons in early age mice are less stable. Axonal growth could expand the mean IBI as new boutons are yet to form and existing boutons are more likely to degenerate. Slower addition and proliferation of TUAs would bring down the mean IBI as established axons with stable bouton densities would have a larger influence in IBI counts. Rapid change in the cognition of young animals and humans is well studied, and these findings may give some insight into the physiological basis behind that change.

IBI is known to vary greatly among hippocampal axons, but we have found that IBI variation remains approximately even across all ages. The coefficient of variation averaged to 0.40 and did not significantly change with age. A value of 1.0 represents a Poisson point process of the spacing of boutons while 0 represents no variation, so our result reflects a sub-random spatial distribution of boutons. CV is calculated by dividing the standard deviation by the mean. Since

standard deviation of IBI increases linearly with mean, it is a valid measure to use for all ranges of IBI (Shepherd & Raastad 2002). Although there is limited information regarding change in the variability of IBI, the presence of a spatial pattern is plausible despite high IBI variability. Some studies have found existing patterns in the variation of bouton spacing, such as an increase in the CV of axons with increasing mean IBI and a decrease in IBI in proximal portions of axons (Pichitpornchai 1994; Shepherd & Raastad 2002). Most axons in our study had a mean IBI between 2 and 10μm, but the strict selection criteria introduce a bias towards larger than actual values. Prior findings with relatively similar measured varicosity spacing support our own of conclusions of IBI variability and length range. Using similar imaging methods, a 2.6 to 9.9μm varicosity spacing range was found in cerebellar axons, with CV's ranging from 0.5 for the lowest mean IBI axons and 0.8 for the highest (Shepherd & Raastad 2003). The bouton selection criteria were less strict than those in our study, introducing a bias opposite to our own towards lower values. An electron microscopy study modeling the three-dimensional structures of hippocampal CA1 and CA3 axons in rats also reveals a wide intervaricosity spacing range of 1.2 to 7μm (Shepherd & Harris 1998). While this finding includes a much smaller sample size, the study uses a more thorough imaging technique which likely reduces counting error. The CV would not change with IBI range skew resulting from methodological choice, as it is a relative measure. Consistent findings of significantly sub-random CV values support semi-ordered bouton distribution as a uniform characteristic of TUAs, establishing some indication of CV as a potential indicator of data quality. The sub-random spatial distribution of boutons and similar observed IBI's indicate some physiological pressure towards a defined morphological pattern. Total TUA length from CA3 cells can range from 150 to 300mm and make synapses with 30,000-60,000 other neurons (Li 1994).

Changes in the variation of bouton spacing may alter the synaptic connectivity map, possibly leading to widespread and distant effects on neural signaling.

The autocorrelation, which eliminates the subjective bouton size threshold bias by removing the need for peak identification, supports the conclusion of an age-related decreasing mean IBI by revealing a slower climb with distance in normalized profile correlation from negative to zero. This represents a higher likelihood of encountering a bouton over a shorter distance from the previous bouton in older mice. The high variability in IBI between axons reduces the analytical strength of the autocorrelation, however it is still useful to confirm general trends in the data. A functional consequence of an increased probability of encountering a bouton along an axon would be lower action potential conduction velocity via propagation delays at varicosities, affecting the dynamics of neural circuitry (Bennett 2009; Manor 1991). An action potential traveling through an axon of an older mouse would be likely to pass through more boutons, slowing the speed of afferent signals. Normal age-related degeneration of hippocampal grey matter is correlated with slower performance in cognitive tests (Papp 2013). Slower action potential propagation speed due to decreased IBI may be a physiological factor in this observed cognitive decline.

We found that boutons of hippocampal TUAs are on average 4.09 times wider than the axon shaft and that bouton size significantly increases with age. No other studies have observed a bouton size change with age, but similar findings of mean bouton size help validate our results. Boutons have been observed to typically be less than 1μm in diameter, which corresponds to a maximum relative size of approximately 5.9 when calculated using the observed mean shaft diameter of 0.17μm (Shepherd 1998). A previously observed pattern in bouton size is an increase in diameter with increasing proximity to the cell body (Pichitpornchai 1994; Shepherd & Raastad, 2003). Interestingly, boutons are also more abundant in proximal locations of the axon as described

above. Considering our previously described results, axons of older mice would have larger and more boutons close to the cell body. Multisynaptic boutons are typically larger than single synapse boutons (Pichitpornchai 1994). Older axons therefore would have a greater number of synapses than younger axons, especially in proximal portions of axons. Logically, the greater synaptic density facilitated by larger boutons comes with the cost of higher resource requirements, as more lipids, proteins, and ATP would be required to build and maintain the synapses. On the other hand, the greater volume of the boutons would increase storage capacity of boutons, helping to offset resource costs.

Lack of Morphological Change with Age in the Neocortex

We found no significant morphological changes with age in axons of the neocortex. The mean IBI for all neocortical axons was 6.1µm, which is within two standard deviations of the hippocampal mean IBI of 4.5 µm. This indicates that the TUAs found in the neocortex have similar *en passant* bouton organization to those found in the hippocampus. Mean IBI did not significantly change have age, but there was an upward trend. Although this conflicts with the correlation found in hippocampal axons, the sample size for neocortical axons was much smaller. Our hippocampal results, including the CV and bouton size findings, are therefore more reliable. The trend IBI found in this axon population may be an exacerbating factor in known mechanisms of age-related neuronal degeneration. Excessive activation of glutamatergic receptors, including NMDA and AMPA, causes Ca^{2+} influx and reactive oxygen species production. This leads to post-synaptic excitotoxicity that might result in dendrite damage or cell death (Mattson 2003). Ca^{2+} is known to cause cell death and degeneration in excess concentration, especially in older neurons (Choi 1985). Theoretically, a high mean IBI in an axon would lead to shortening of sustained high-frequency excitatory action potentials due to impaired ion diffusion, which may alleviate some excitotoxicity.

Conversely, the impaired diffusion and lower volume resulting from reduced S/V could also increase likelihood of Ca^{2+} toxicity. The concentration of Ca^{2+} would have larger fluctuations, and the ions would take longer to diffuse to mitochondria in the axon that contribute to sequestering Ca^{2+} (Toescu 2004). Hippocampal axons demonstrate a notable sensitivity to Ca^{2+}, indicating that other mechanisms are likely to be more significant factors in age-related excitotoxicity than increased IBI. CA1 cells have increased Ca^{2+} dependent afterhyperpolarizations with age and both CA1 and CA3 have little to none of Ca^{2+}-binding protein calbindin (Sloviter 1989; Toescu 2004).

The CV of neocortical axons show a trend towards increase that was close to significant ($p = 0.084$). The mean CV of 0.47 was similar to 0.40 found in hippocampal axons. This consistency supports our conclusion that the boutons of TUAs follow a sub-random pattern of spatial distribution. The upward trend of neocortical bouton CV was stronger than the downward trend of hippocampal bouton CV. We found a downward and non-significant trend in relative bouton size of neocortical axons. The mean relative bouton size ratio was 2.63, which is smaller than the hippocampal ratio of 4.09. Cortical axons undergo synaptogenesis and frequent turnover of *en passant* boutons (De Paola 2006; Stettler 2006). If bouton turnover rate is higher than in hippocampal axons, then neocortical boutons may not remain long enough to grow larger and the spatial distribution of boutons may vary more. This would help to explain the differences between hippocampal and neocortical axons in CV and relative bouton size, however this still leaves questions about homogeneity in structure between the two types of axons.

Methodological Considerations

The use of varying methodology allowed us to flexibly examine age-related change in the bouton organization of thin unmyelinated axons. We found several procedural strategies that result

in superior data production, but different approaches came with their own advantages and disadvantages.

Staying in the hippocampus during fluorescent imaging with 100X magnification proved to be difficult. In the prior studies from our lab DAPI was used to label the DNA of cells throughout the tissue in conjunction with DiI axon labelling, producing a fluorescent emission landscape of a different wavelength that was useful for navigation. DAPI was not available for this study, so tissues were only labelled with DiI. Since DiI is distributed across the slice at random points rather than a whole-tissue stain, there were few visual cues that indicated where in the sample the lens was aimed. Emitted light also provided few visual cues at maximum magnification. In the case of DiI-exclusive labelling, after finding the desired region using lower magnifications, navigation using fluorescence at 100X magnification was based on estimation of the location of the focal point after movement. The hippocampus was easy to locate using lower magnifications on either emitted or excitation light but 100X magnification lens required oil immersion, making returning to lower magnifications for navigation non-viable. The first few axons were likely to be hippocampal, however straying away from the hippocampal area during the search for axons was inevitable. The neocortex was easier to navigate by locating the outer edge of the cortex and searching inwards. Localization cues obtained from the use of DAPI would be an advantage in future studies. The Keyence software came with a helpful navigation software but did not have a 100X lens, so finding the right combination of equipment is important for precise imaging. Perhaps the most significant disadvantage with our imaging method was the limited length of axon we could capture in one image. Stitching multiple images of the same axon is possible but cumbersome, introducing the risk of repeated or omitted data.

DiI was an extremely effective labeling method for our purposes. The ability to randomly spread crystals across the sample allowed us to label only the membranes that touched the crystal rather than the entire sample. This resulted in sparse labeling of axons that fluoresce brightly against a dark background. The most difficult step is choosing how much DiI to use. Because of how little crystal is needed to dye the samples, the mass of the required amount cannot be precisely measured and must be estimated by eye. Figure 11 compares 20X images of slices showing either high or suitable crystal density. The simplicity and reasonable reproducibility of DiI labelling allows rapid production of data, which is necessary for the high sample size requirements of our study. Other labeling methods include Golgi staining and viral green fluorescent protein (GFP) labelling. GFP labelling produces bright and targeted labelling of fine neuronal processes like axons, however it requires modification to its coding sequence and can only be used in living tissue (Moriyoshi 1996). Golgi staining has been used for over a century and provides relatively sparse labelling of axons but requires multiple applications of osmium-dichromate over the course of several days (Valverde 1970). Electron microscopy can also be used to examine axon morphology in much greater detail than fluorescent microscopy methods. However, this method currently restricts the observable dimensions of samples, is extremely time consuming, and requires equipment that is more difficult to access and operate. DiI is far less labor-intensive than any of these methods and produces samples that are more than adequate for gathering data.

We found that both fresh slices and slices preserved with paraformaldehyde were effectively labelled with DiI. Although paraformaldehyde has been found to cause varying degrees of shrinkage in our study and others, relative measurements like CV and relative bouton size are not affected (Kirov 1999). We experimented with sodium azide and potassium permanganate as discussed previously, but neither produced samples that were viable for DiI

labelling and imaging. A lower concentration of sodium azide, perhaps 0.1% as used in the Minassian study, would likely produce better samples. Fresh slices may produce mean IBI counts that are closer to the actual value compared to slices preserved with paraformaldehyde, however this requires closer examination.

Future Directions

The data produced by this study are not definitive representations of morphological change with age, however clear patterns in the hippocampal axon morphology and similar morphological features of neocortical axons are enough to motivate future studies. Since morphology varies between axons, studying their morphology demands large amounts of data. A direct improvement to our study would be to supplement hippocampal data with axons from mice between 200-500 days old. Mice of earlier ages have a stronger influence on mean values and their trends in our data set, making our conclusions less relevant to older age groups. The neocortical data also come from a clustered age group and would benefit from more data. The size of boutons had unclear implications. There is a lack of knowledge regarding the direct consequences of differing morphology. Future studies of axons *in vivo* or axon simulations determining the relationships between bouton size and synaptic properties, IBI and characteristics of action potential propagation, or bouton variance and neural connectivity would elucidate much about the physiological significance of the trends we observed. Our understanding of how morphological change in TUAs affects cognition is almost nonexistent. A more direct way to measure the correlation between cognition and axon morphology, such as a comparison among mice between their cognitive ability and overall axonal morphology profiles in relevant cortical regions, would be useful to determine behavioral and cognitive consequences of certain morphological features.

Graphs and Figures

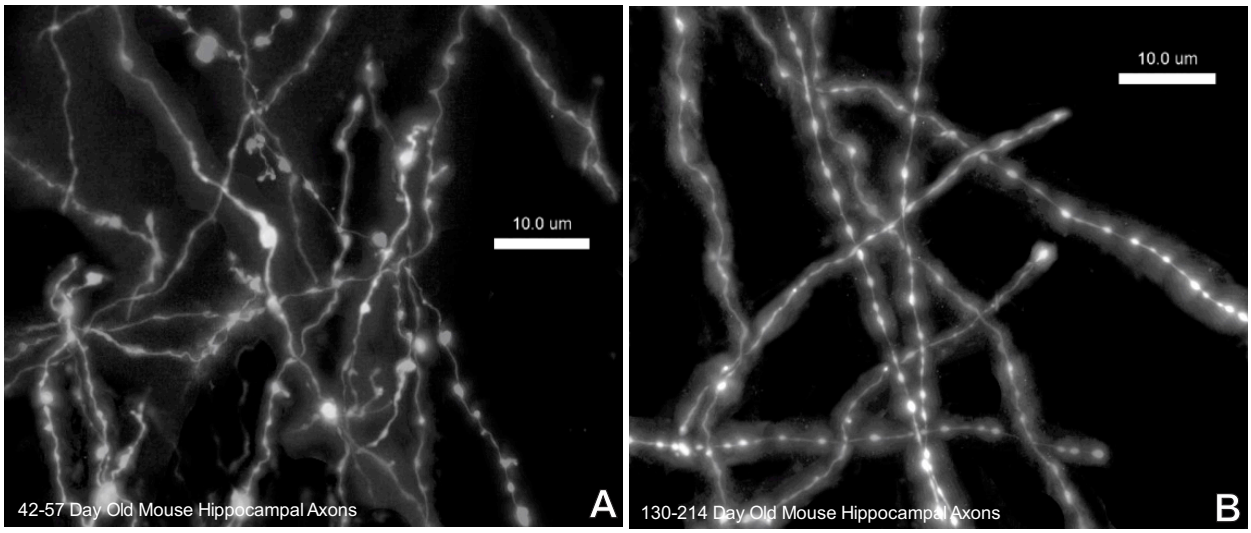

Figure 1: A. Hippocampal axons from paraformaldehyde-preserved brains of 57-day old, 50-day old, and 42-day old mice. **B.** Hippocampal axons from paraformaldehyde-preserved brains of 161-day old, 130-day old, 214-day old, 226-day old, and 146-day old mice. Two collages of individual axons found in multiple slices grouped by 'young' and 'old' mice. Images were processed (subtract background, z-project, convert to 16-bit) and individual axons picked out and arranged.

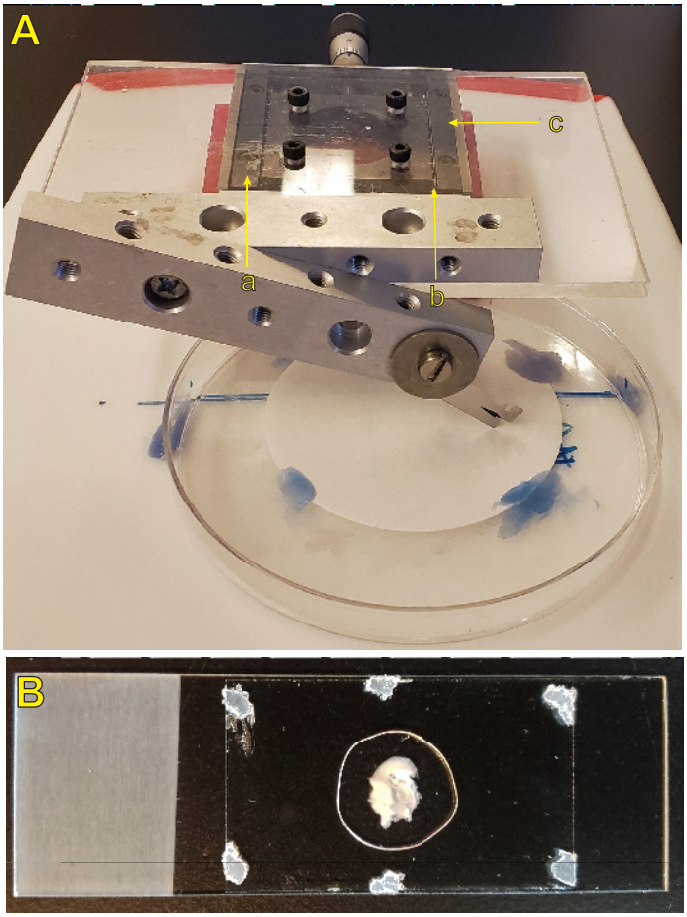

Figure 2: A. The slicing device. The screw mechanism is seen behind the acrylic platform. The platform is screwed onto a frame through which rails attached to the base are threaded at the bottom. The frame is securely attached to the base and rests on ball bearings to allow movement. In the picture, you can see the frame (**a**), thin fissures revealing the ball bearings (**b**), and the base (**c**). The screwing mechanism moves a rod that pushes against the frame. Two springs on the opposite side of the frame push back, allowing the frame to follow the rod when retracted. The blade is pinched in between the two-piece metal frame and a screwed in washer. The washer can be loosened to adjust blade angle, and the handle loosened to adjust blade height. The handle simply rests on top of the acrylic platform and is slid back and forth.
B. An example of a sample slide. 6 dabs of mounting paste are pressed between the cover glass and the slide, and a slice is seen in the middle submerged in a modest amount of glycerol.

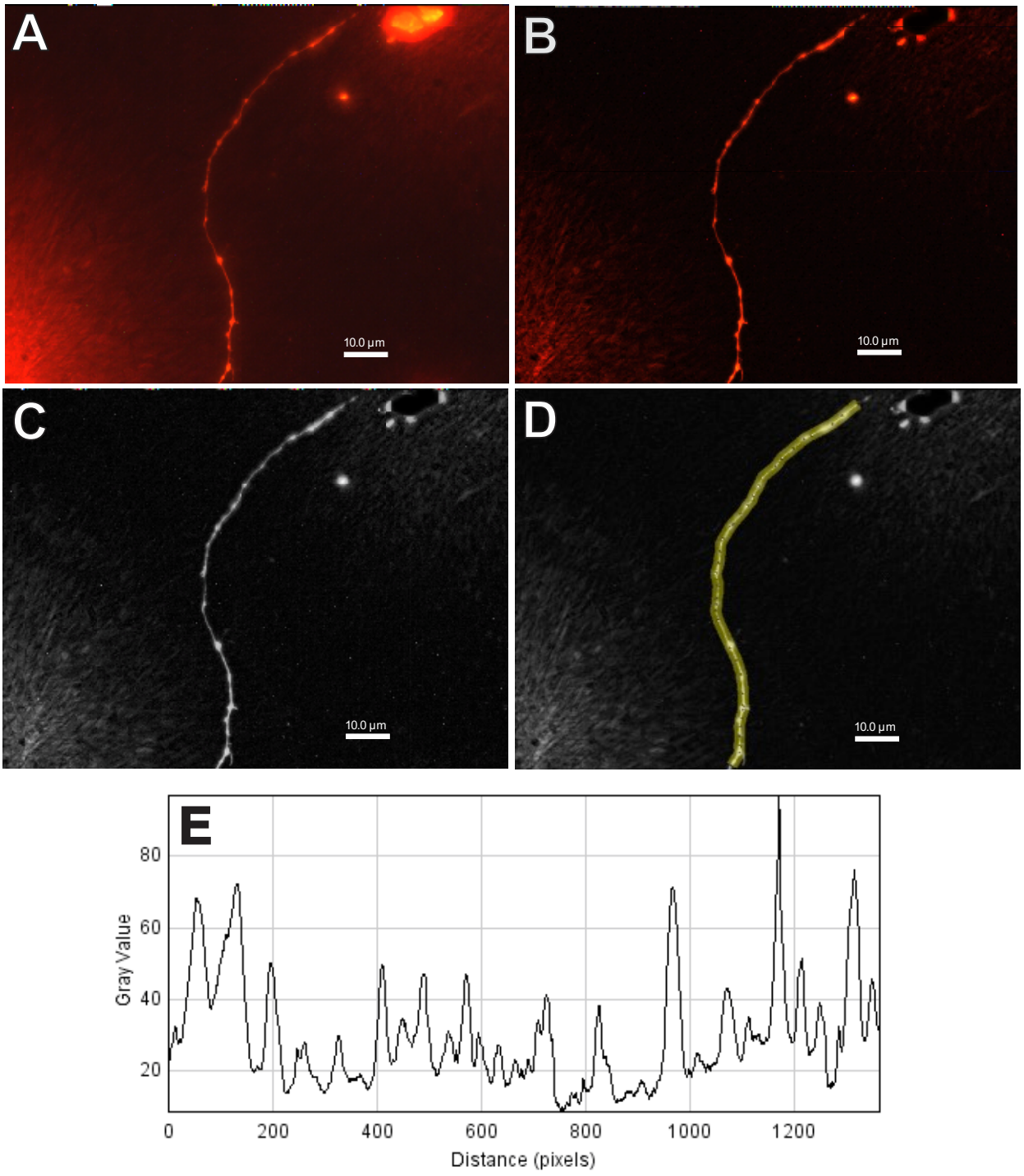

Figure 3: The progression through image processing of a neocortical axon from the fresh brain of a159-day-old mouse and the resulting data. **A:** Z-projected image. **B:** Image A with background emission subtracted. **C:** Image B converted to 16-bit greyscale. **D:** 35-pixel wide segmented line highlighting the axon to be analyzed. **E:** Raw contrast profile plot extracted from along the yellow line.

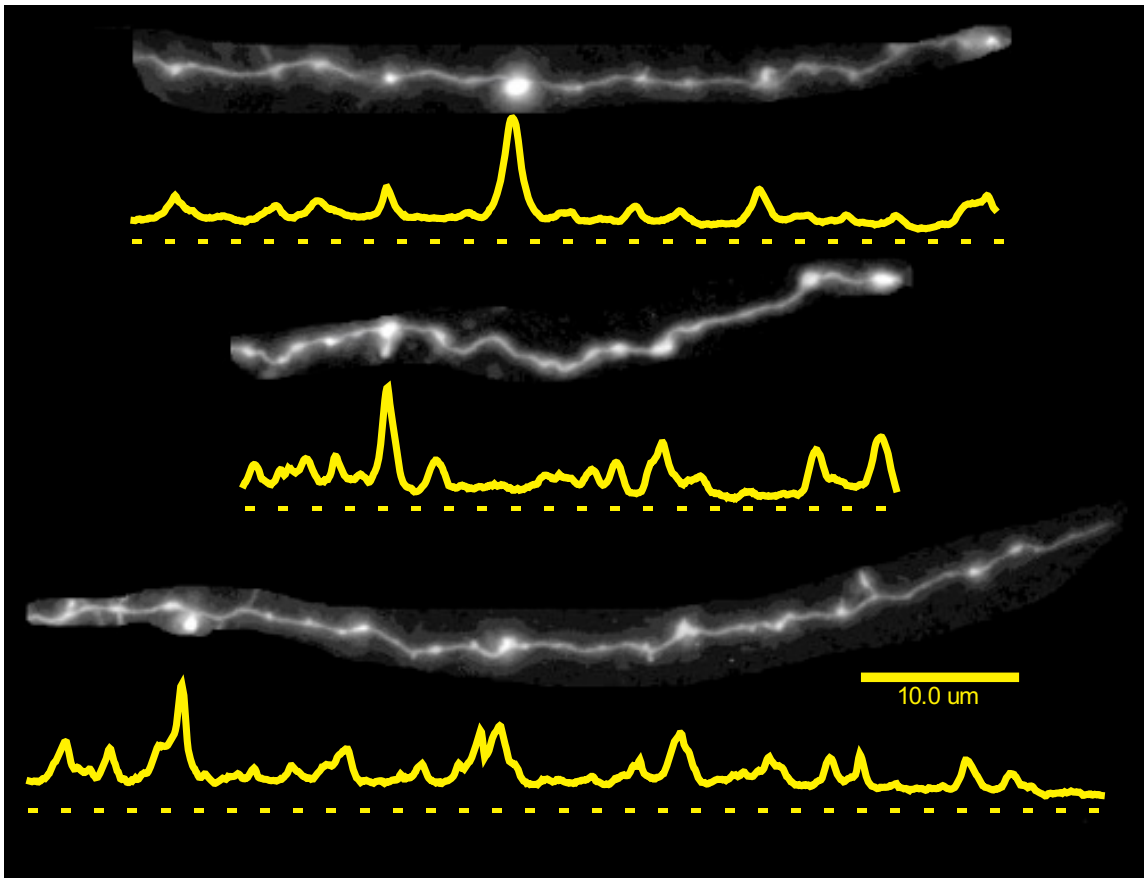

Figure 4: Examples of normalized contrast profile plots of hippocampal cells of 57-day-old mice. These axons are from a sample preserved with paraformaldehyde. The profiles are matched to the length of the axon, illustrating how the luminosity is translated into the contrast profile.

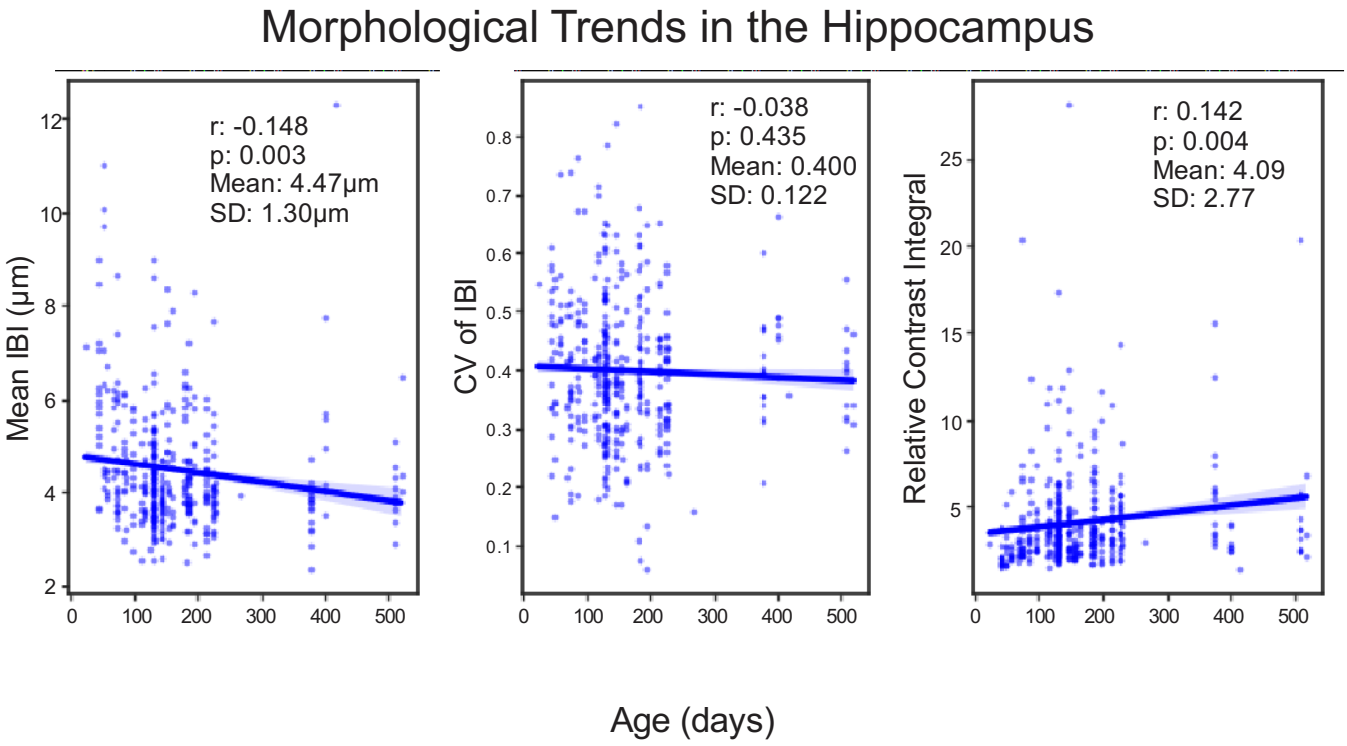

Figure 5: Graphs containing the mean inter-bouton interval, coefficient of variation, and relative contrast integral (bouton size) for all hippocampal axons (n = 416). Linear correlation lines show a decrease in mean IBI and an increase in bouton size with age, but no change in CV. The highlighted area indicates the 95% confidence interval of the regression line.

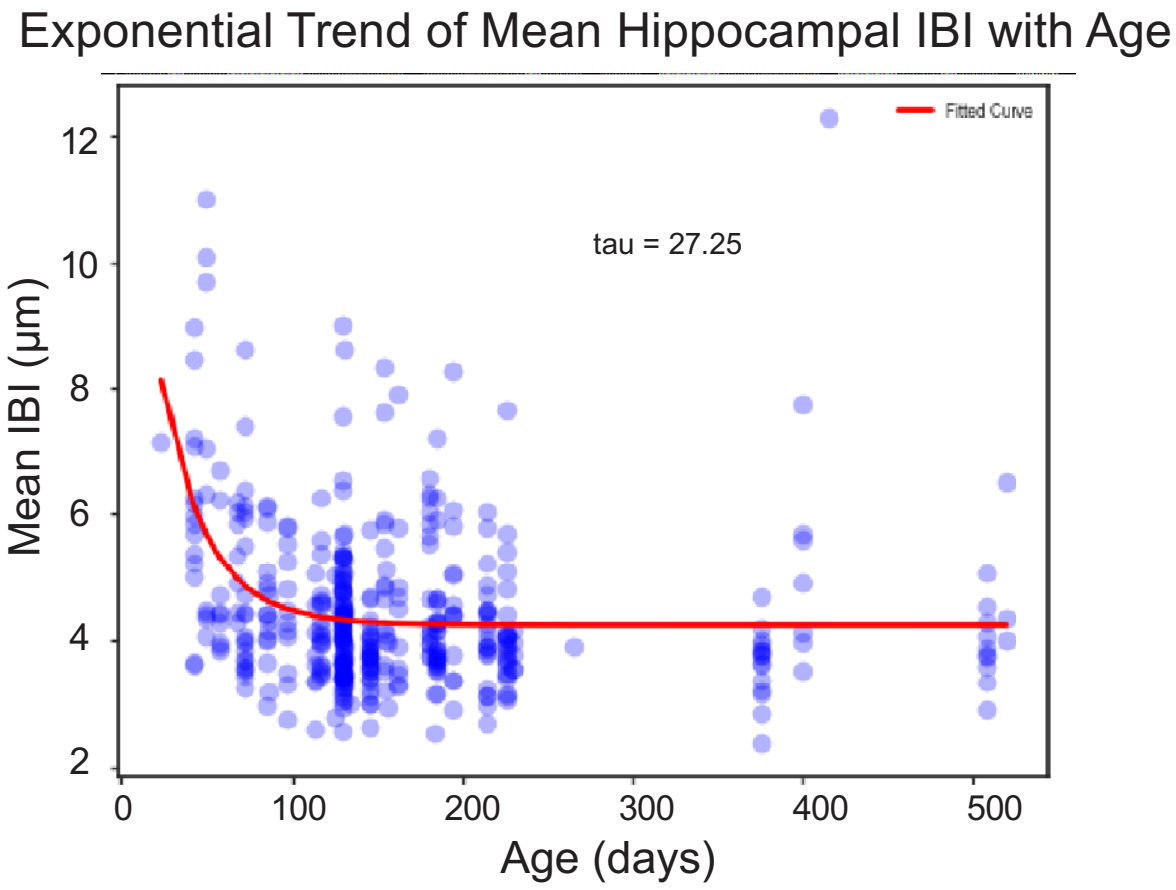

Figure 6: An exponential curve fitted over mean IBI data from individual hippocampal axons (n = 416). There is a sharp decrease of mean IBI that slows exponentially, beginning to plateau between 100 and 140 days of age. The tau value indicates that decrease in IBI slows to 36.8% of its value about every 27 days. The paucity of data from mice over 250 days of age makes the curve less reliable for older mice.

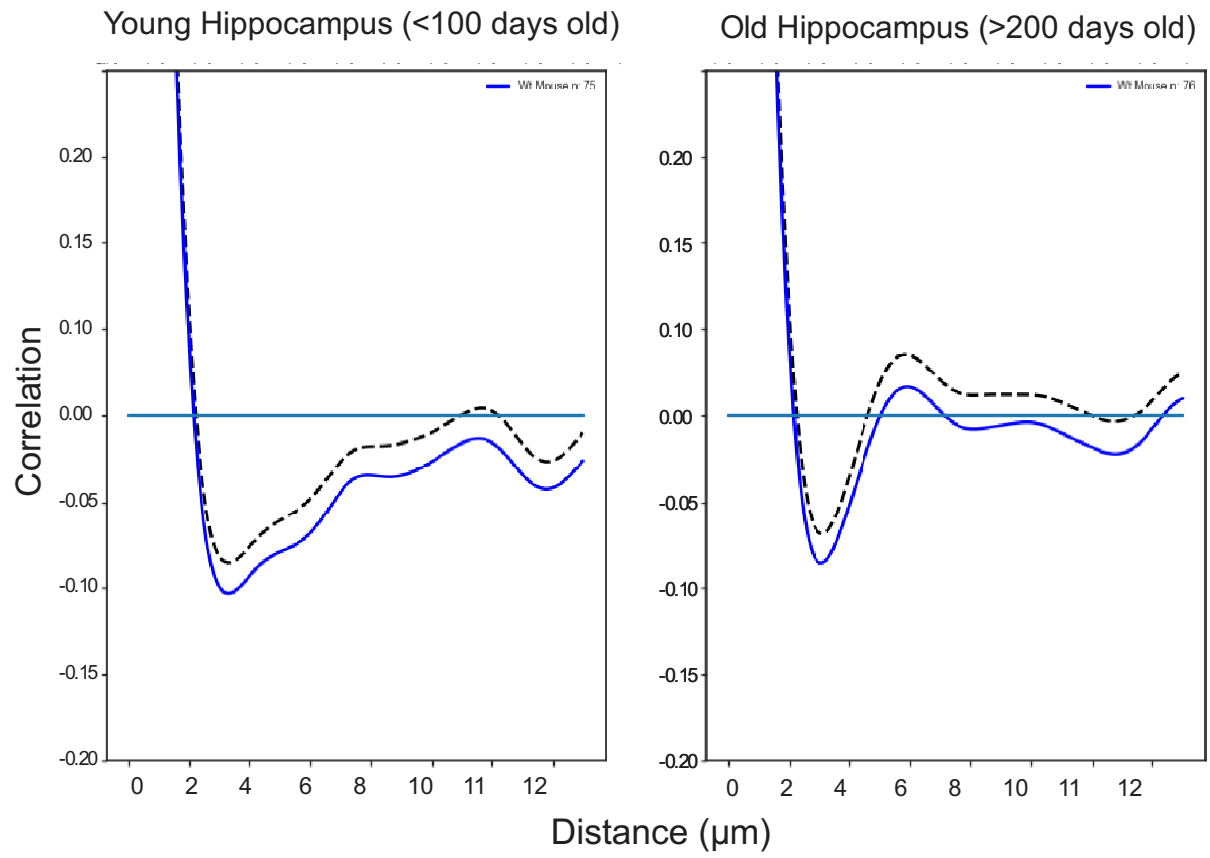

Figure 7: An autocorrelation of raw hippocampal axon profile data (example shown in Figure 3e). The lagging curve of old mice becomes less negatively correlated at a shorter distance.

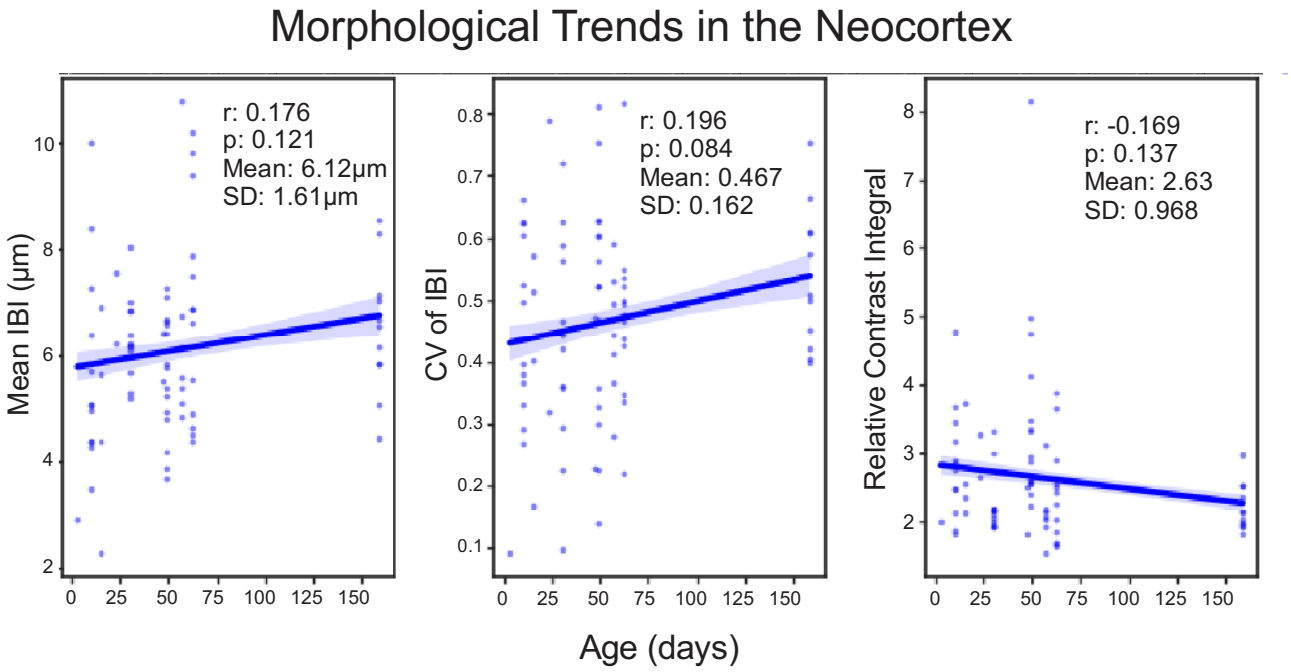

Figure 8: Plots showing the same data as Figure 5 but with neocortical axons instead of hippocampal axons (n = 79). Linear regression lines show no significant change of any parameter with age. The observed non-significant trends are inverse to the significant trends of hippocampal axons.

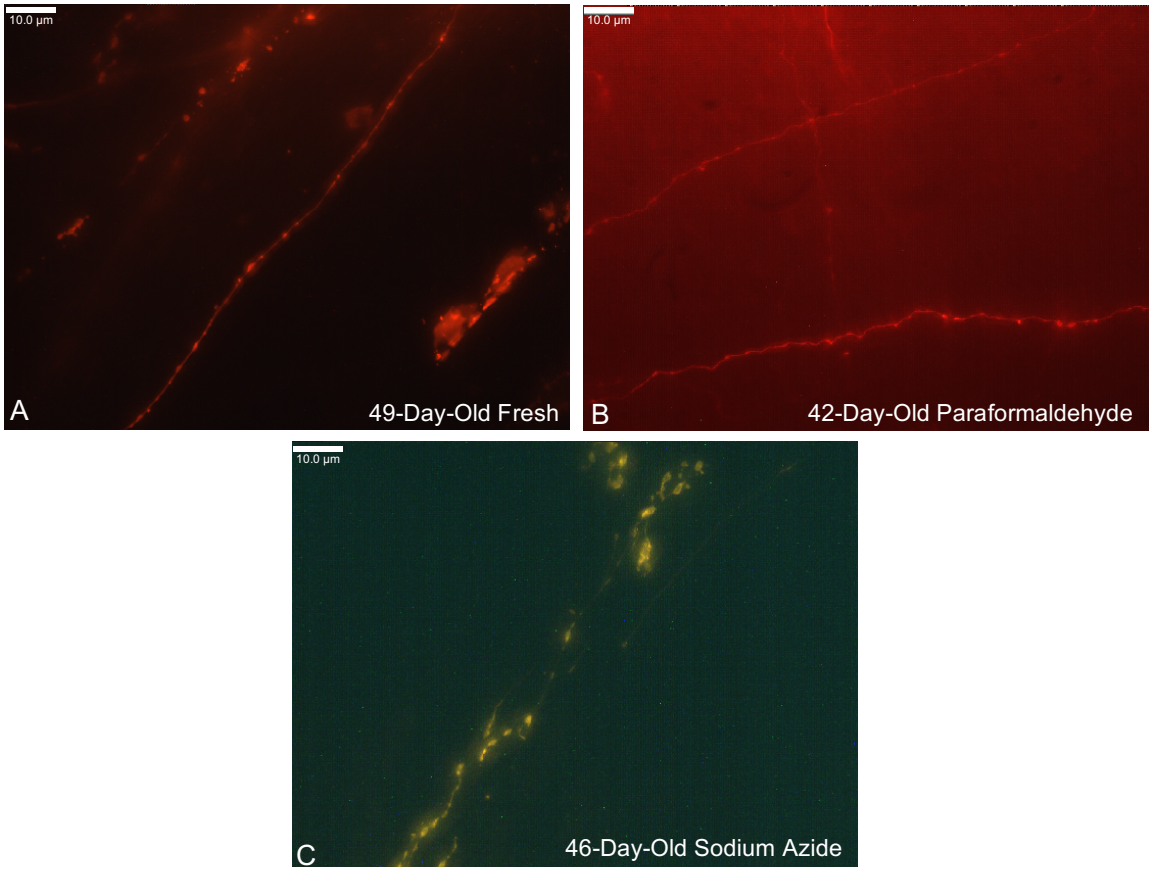

Figure 9: A: Neocortical axons from a fresh, 49-day-old slice. **B:** Hippocampal axons from a PFA-preserved, 42-day-old slice. **C:** Hippocampal axon from sodium azide-preserved, 46-day-old slice. Comparison of raw image (i.e. no background subtraction or greyscale conversion) z-projections between a fresh slice and slices preserved with either paraformaldehyde or sodium azide. Fresh and PFA axons are labelled well and relatively equally, but the PFA slice shows much more background emission. Sodium azide did not label well and produced excessive background emission.

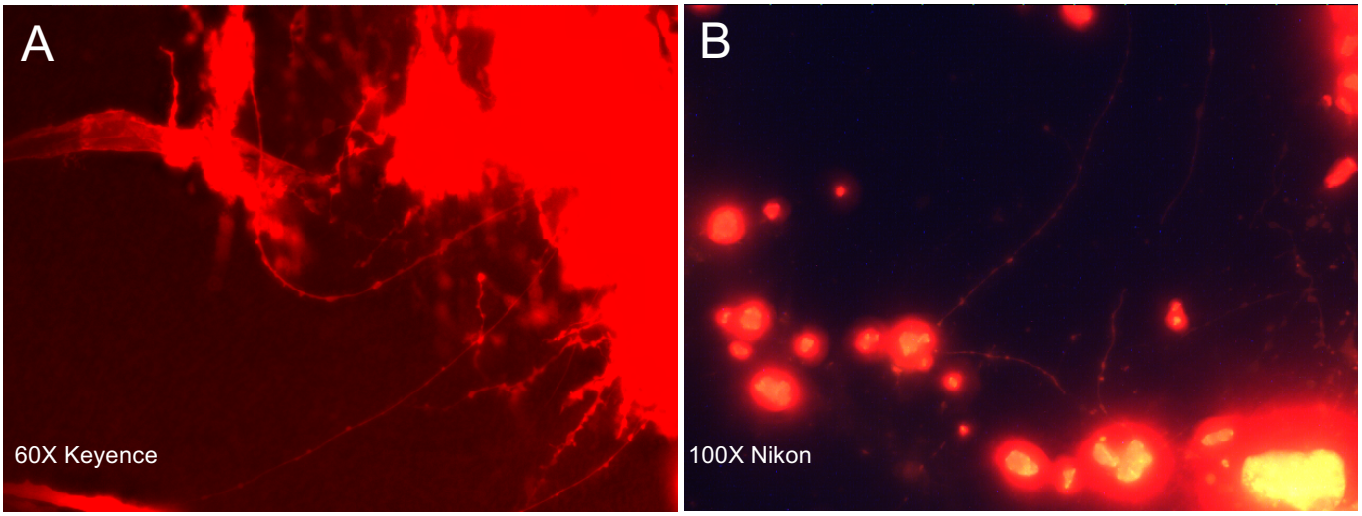

Figure 10: Comparison between a 60X image from the Keyence (**A**) and a 100X image from the Nikon (**B**). The Keyence had a higher native resolution and produced sharper images, but there is more background emission, likely due to the different excitation wavelengths of the filters. Both images were taken from fresh slices.

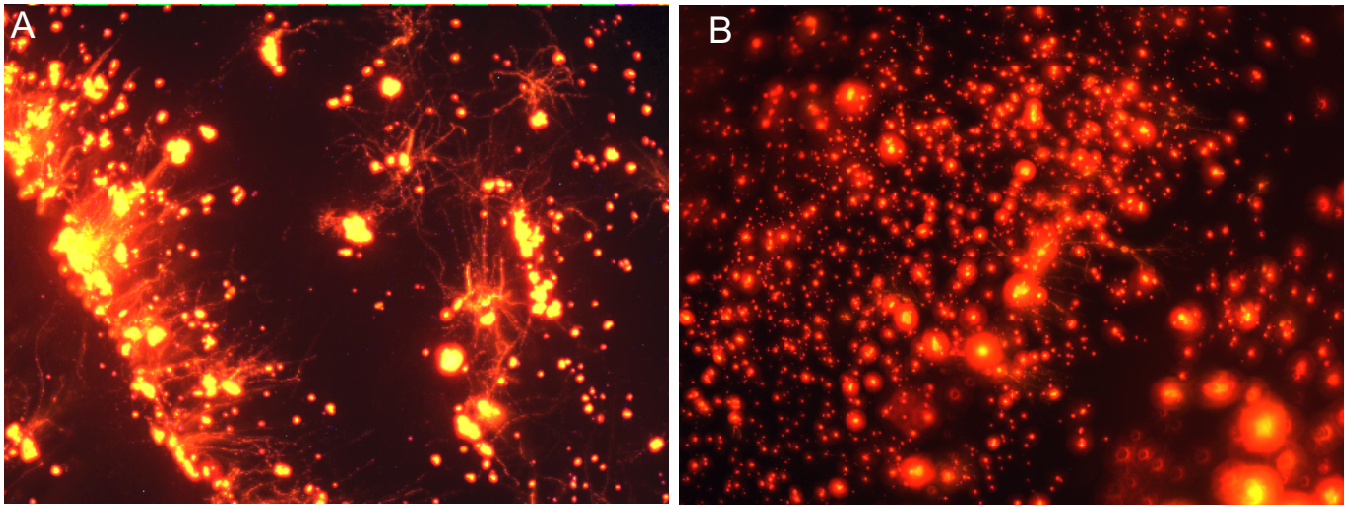

Figure 11: Two 10X magnification showing the difference between **A:** sparse labelling and **B:** excessive labelling in fresh slices. Sparse labelling leads to much lower background emission and clearer views of axons.

References

Adams MM, Donohue HS, Linville MC, Iversen EA, Newton IG, Brunso-Bechhtold JK (2010) Age-related synapse loss in hippocampal CA3 is not reversed by caloric restriction. Neuroscience, 171(2), 373–382.

Andersen P (1975) Organization of Hippocampal Neurons and Their Interconnections. The Hippocampus, 155–175.

Anderson JC, Martin KAC (2001) Does bouton morphology optimize axon length? Nature Neuroscience, 4(12), 1166–1167.

Barnes CA, Rao G, Orr G (2000) Age-Related Decrease in the Schaffer Collateral-Evoked EPSP in Awake, Freely, Behaving Rats. Neural Plasticity, 7(3), 167–178.

Bennett CB, Muschol M (2009) Large Neurohypophysial Varicosities Amplify Action Potentials: Results from Numerical Simulations. Endocrinology, 150(6) 2829-2836.

Chase MH, Engelhardt JK, Adinolfi AM, Chirwa SS (1992) Age-dependent changes in cat masseter nerve: an electrophysiological and morphological study. Brain Research 586(2), 279–288.

Cheng C, Trzcinski O, Doering LC (2014) Fluorescent labeling of dendritic spines in cell cultures with the carbocyanine dye "DiI". Frontiers in Neuroanatomy, 8.

Choi DW (1985) Glutamate neurotoxicity in cortical cell culture is calcium dependent. Neuroscience Letters, 58(3), 293–297.

Coleman M (2005) Axon degeneration mechanisms: commonality amid diversity. Nature Reviews Neuroscience, 6(11), 889–898.

Colby S, Ortman JM (2015) Projections of the Size and Composition of the U.S. Population: 2014 to 2016. US Census Bureau.

Courchesne E, Chisuum GJ, Townsend J, Cowles A, Covington J, Egaas B, Harwood M, Hinds S, Press GA (2000) Normal Brain Development and Aging: Quantitative Analysis at in Vivo MR Imaging in Healthy Volunteers. Radiology, 216(3), 672-682.

De Paola V, holtmaat A, Knott G, Song S, Wilbrecht L, Caroni P, Svoboda K (2006) Cell Type-Specific Structural Plasticity of Axonal Branches and Boutons in the Adult Neocortex. Neuron, 49(6), 861–875.

Dobbs AR, & Rule BG (1989) Adult age differences in working memory. Psychology and Aging 4(4), 500–503.

Geinisman Y, de Toled-Morrell L, Morrell F, Persina IS, Rossi M (1992) Age-related loss of axospinous synapses formed by two afferent systems in the rat dentate gyrus as revealed by the unbiased stereological dissector technique. Hippocampus, 2(4), 437–444.

Geinisman Y, Ganeshina O, Yoshida R, Berry RW, Disterhoft JF, Gallagher M (2004) Aging, spatial learning, and total synapse number in the rat CA1 stratum radiatum. Neurobiology of Aging, 25(3), 407–416.

Geng YQ, Guan JT, Xu XH, Fu YC (2010) Senescence-associated beta-galactosidase activity expression in aging hippocampal neurons. Biochemical and Biophysical Research Communications, 396(4), 866–869.

Honig MG, Hume RI (1986) Fluorescent Carbocyanine Dyes Allow Living Neurons of Identified Origin to Be Studied in Long-Term Cultures. The Journal of Cell Biology, 103(1), 171-187.

Jacobs JM, Love S (1985) Qualitative and quantitative morphology of human sural nerve at different ages. Brain, 108(4), 897–924.

Jernigan TL, Archibald SL, Fennema-Notestine C, Gamst AC, Stout JC, Bonner J, Hesselink JR (2001) Effects of age on tissues and regions of the cerebrum and cerebellum. Neurobiology of Aging, 22(4), 581–594.

Kirov SA, Sorra KE, Harris KM (1998) Three-Dimensional Structure and Composition of CA3→CA1 Axons in Rat Hippocampal Slices: Implications for Presynaptic Connectivity and Compartmentalization. The Journal of Neuroscience, 18(20), 8300–8310.

Knoth R, SIngec I, Ditter M, Pantazis G, Capetian P, Meyer RP, Horvat Vo, Volk B, Kempermann G (2010) Murine Features of Neurogenesis in the Human Hippocampus across the Lifespan from 0 to 100 Years. PLoS ONE, 5(1), e8809.

Kuhn H, Dickinson-Anson H, Gage F (1996) Neurogenesis in the dentate gyrus of the adult rat: age-related decrease of neuronal progenitor proliferation. The Journal of Neuroscience 16(6), 2027–2033.

Lazic SE (2012) Modeling hippocampal neurogenesis across the lifespan in seven species. Neurobiology of Aging, 33(8), 1664–1671.

Li XG, Somogyi P, Ylinen A, Buzsáki G (1994) The hippocampal CA3 network: An in vivo intracellular labeling study. Journal of Comparative Neurology 339(2), 181–208.

Lippa AS, Critchett DJ, Ehlert F, Yamamura HI, Enna SJ, Bartus RT (1981) Age-related alterations in neurotransmitter receptors: An electrophysiological and biochemical analysis. Neurobiology of Aging, 2(1), 3–8.

Manor Y, Koch C, Segev I (1991) Effect of geometrical irregularities on propagation delay in axonal trees. Biophysical Journal, 60(6), 1424–1437.

Mattson MP (2003) Excitotoxic and Excitoprotective Mechanisms: Abundant Targets for the Prevention and Treatment of Neurodegenerative Disorders. NeuroMolecular Medicine, 3(2), 65–94.

Minassian H, Huang S (1979) Effect of sodium azide on the ultrastructural preservation of tissues. Journal of Microscopy, 117(2), 243–253.

Mishchenko Y, Hu T, Spacek J, Mendenhall J, Harris KM, Chklovskii DB (2010) Ultrastructural analysis of hippocampal neuropil from the connectomics perspective. Neuron 67(6), 1009-1020.

Moriyoshi K, Richards LJ, Akazawa C, O'Leary DD, Nakanishi S (1996) Labeling Neural Cells Using Adenoviral Gene Transfer of Membrane-Targeted GFP. Neuron, 16(2), 255–260.

Nakayama H, Noda K, Hotta H, Ohsawa H, Hosoya Y (1998) Effects of aging of numbers, sizes and conduction velocities of myelinated and unmyelinated fibers of the pelvic nerve in rats. Journal of the Autonomic Nervous System 69(2-3), 148-155.

Namer B, Barta B, Orstavik K, Schmidt R, Carr R, Schmelz M, Handwerker HO (2009) Microneurographic assessment of C-fibre function in aged healthy subjects. The Journal of Physiology 587(2), 419-428.

Oakley H, Cole SL, Logan S, Maus E, Shao P, Craft J, Guillozet-Bonaarts A, Ohno M, Disterhoft J, Van Eldik L, Berry R, Vassar R (2006) Intraneuronal β-Amyloid Aggregates, Neurodegeneration, and Neuron Loss in Transgenic Mice with Five Familial Alzheimer's Disease Mutations: Potential Factors in Amyloid Plaque Formation. Journal of Neuroscience 26(40), 10129-10140.

Papp KV, Kaplan RF, Springate B, Moscufo N, Wakefield DB, Guttmann CRG, Wolfson L (2013) Processing speed in normal aging: Effects of white matter hyperintensities and hippocampal volume loss. Aging, Neuropsychology, and Cognition, 21(2), 197–213.

Park DC, Reuter-Lorenz P (2009) The Adaptive Brain: Aging and Neurocognitive Scaffolding. Annual Review Psychology 60, 173-196.

Park DC, Smith AD, Lautenschlager G, Earles JL, Frieske D, Zwahr M, Gaines CL (1996) Mediators of long-term memory performance across the life span. Psychology and Aging 11(4), 621–637.

Peters A, ROsene DL, Moss MB, Kemper TL, Abraham CR, Tigges J, Albert MS (1996) Neurobiological Bases of Age-Related Cognitive Decline in the Rhesus Monkey. Journal of Neuropathology & Experimental Neurology, 55(8), 861–873.

Phillip JM, Wu P, Gilkes DM, Williams W, McGovern S, Daya J, Chen J, Aifuwa I, Lee JSH, Fan R, Walston J, Wirtz D (2017) Biophysical and biomolecular determination of cellular age in humans. Nature Biomedical Engineering, 1(7), 0093.

Pichitpornchai C, Rawson JA, Rees S (1994) Morphology of parallel fibres in the cerebellar cortex of the rat: An experimental light and electron microscopic study with biocytin. The Journal of Comparative Neurology, 342(2), 206–220.

Qiao Q, Ma L, Li W, Tasi JW, Yang G, Gan WB (2015) Long-term stability of axonal boutons in the mouse barrel cortex. Developmental Neurobiology, 76(3), 252–261.

Raastad M, Shepherd GMG (2004) Single-axon action potentials in the rat hippocampal cortex. The Journal of Physiology 548(3), 145-152.

Reeve A, Simcox E, Turnbull D (2014) Ageing and Parkinson's disease: Why is advancing age the biggest risk factor? Ageing Research Reviews 14(100), 19-30.

Reitz C, Brayne C, Mayeux R (2011) Epidemiology of Alzheimer disease. Nature Reviews Neurology 7(3), 137-152.

Salthouse T (2009) When does age-related cognitive decline begin? Neurobiology of Aging 30(4), 507-514.

Shepherd GMG, Harris KM (1998) Three-Dimensional Structure and Composition of CA3→CA1 Axons in Rat Hippocampal Slices: Implications for Presynaptic Connectivity and Compartmentalization. Journal of Neuroscience 18(20), 8300-8310.

Shepherd GMG, Raastad M, Anderson P (2002) General and variable features of varicosity spacing along unmyelinated axons in the hippocampus and cerebellum. PNAS 99(9), 6340-6345.

Sloviter RS (1989) Calcium-binding protein (calbindin-D28k) and parvalbumin immunocytochemistry: Localization in the rat hippocampus with specific reference to the selective vulnerability of hippocampal neurons to seizure activity. The Journal of Comparative Neurology, 280(2), 183–196.

Small SA, Tsai WY, DeLaPaz R, Mayeux R, Stern Y (2002) Imaging hippocampal function across the human life span: Is memory decline normal or not? Annals of Neurology, 51(3), 290–295.

Smalls SL, Okere CO (2012) Acute restraint increases varicosity density and reduces the inter-varicosity distance in NADPH diaphorase-containing neurons in the rat dorsolateral periaqueductal gray matter. Neuroscience Letters, 511(1), 23-27).

Sorra K, Harris KM (1993) Occurrence and three-dimensional structure of multiple synapses between individual radiatum axons and their target pyramidal cells in hippocampal area CA1. The Journal of Neuroscience, 13(9), 3736–3748.

Stepanyants A, Hof PR, Chkovskii DB (2002) Geometry and Structural Plasticity of Synaptic Connectivity. Neuron, 34(2), 275–288.

Stettler DD, Yamahachi H, Li W, Denk W, Gilbert CD (2006) Axons and Synaptic Boutons Are Highly Dynamic in Adult Visual Cortex. Neuron, 49(6), 877–887.

Svennerholm L, Boström K, Jungbjer B (1997) Changes in weight and compositions of major membrane components of human brain during the span of adult human life of Swedes. Acta Neuropathologica 94(4), 345–352.

Terribilli D, Schaufelberger MS, Duran FLS, Zanetti MV, Curiati PK, Menezes PR, Scazufca M, Amaro Jr. E, Leite C, Busatto GF (2011) Age-related gray matter volume changes in the brain during non-elderly adulthood. Neurobiology of Aging, 32(2), 354–368.

Terry RD, DeTeresa R, Hansen LA (1987) Neocortical cell counts in normal human adult aging. Annals of Neurology 21(6), 530–539.

Todd ME, Tokito MK (1981) Improved Ultrastructural Detail in Tissues Fixed with Potassium Permanganate, Stain Technology, 56:6.

Toescu EC, Verkhratsky A, Landfield PW (2004) Ca2+ regulation and gene expression in normal brain aging. Trends in Neurosciences, 27(10), 614–620.

Valverde F (1970) The Golgi Method. A Tool for Comparative Structural Analyses. Contemporary Research Methods in Neuroanatomy, 12-31.

Verdú E, Ceballos D, Vilches JJ, Navarro X (2008) Influence of aging on peripheral nerve function and regeneration. Journal of the Peripheral Nervous System, 5(4), 191–208.

Witte, Kenneth L, Freund, Joel S, Sebby, Rickard A (1990) Age differences in free recall and subjective organization. Psychology and Aging 5(2), 307-309.

Zehr JL, Nichols LR, Schulz KM, Sisk CL (2008) Adolescent development of Neuron Structure in Dentate Gyrus Granule Cells of Male Syrian Hamsters. Developmental Neurobiology, 68(14), 1517-1526.